Characterization and quantification of natural and anthropogenic titanium-containing particles using single-particle ICP-TOFMS

Hark Karkee[1,a] and Alexander Gundlach-Graham[1,b]*

1. Department of Chemistry, Iowa State University, Ames, Iowa, 50011, United States;

a. orcid.org/0000-0002-4588-8512

b. orcid.org/0000-0003-4806-6255

*Address correspondence: alexgg@iastate.edu

Abstract

Titanium-containing nanoparticles (NPs) and sub-micron particles (μPs) in the environment can come from natural or anthropogenic sources. In this study, we investigate the use of single-particle inductively coupled plasma time-of-flight mass spectrometry (spICP-TOFMS) to measure and classify individual Ti-containing particles as either engineered (Ti-eng) or naturally occurring (Ti-nat) based on elemental composition and multi-element mass ratios. We analyze mixtures of four Ti-containing particle types: anthropogenic food-grade TiO_2 particles and particles from rutile, ilmenite, and biotite mineral samples. Through characterization of neat particle suspensions, we develop a decision-tree-based classification scheme to distinguish Ti-eng from Ti-nat particles, and to classify individual Ti-nat particles by mineral type. Engineered TiO_2 and rutile particles have the same major-element composition. To distinguish Ti-eng particles from rutile, we develop particle-type detection limits based on the average crustal abundance ratio of titanium to niobium. For our measurements, the average Ti mass needed to classify Ti-eng particles is 9.3 fg, which corresponds to a diameter of 211 nm for TiO_2. From neat suspensions, we demonstrate classification rates of 55%, 32%, 75%, and 72% for Ti-eng, rutile, ilmenite, and biotite particles, respectively. Our classification approach minimizes false-positive classifications, with rates below 5% for all particle types. Individual Ti-eng particles can be accurately classified at the sub-micron size range, while the Ti-nat particles are classified in the nano-regime (diameter < 100 nm). Efficacy of our classification approach is demonstrated through the analysis of controlled mixtures of Ti-eng and Ti-nat and the analysis of natural stream water spiked with Ti-eng particles. In control mixtures, Ti-eng particles can be measured and classified at particle-number concentrations (PNCs) 60-times lower than that of Ti-nat particles and across a PNC range of at least three orders of magnitude. In the stream water sample, Ti-eng particles are classified at environmentally relevant PNCs that are 44-times lower than the background Ti-nat PNC and 2850-times lower than the total PNC.

Keywords

nanoparticles, sub-micron particles, titanium nanoparticles, anthropogenic particles, natural particles, single-particle ICP-TOFMS, particle classification, particle-type detection limits, single-particle minerology, online microdroplet calibration

Synopsis

Our study reports a method for classification and quantification of individual anthropogenic and natural titanium nanoparticles and sub-micron particles at environmentally relevant concentrations in controlled Ti-mineral mixtures and in stream water.

Introduction

The detection and classification of naturally occurring and anthropogenic nanoparticles (size < 100 nm) and sub-micron particles (size < 1 µm) in environmental samples is an area of active research and analytical method development.[1] The characterization of individual nanoparticles (NPs) and sub-micron particles (µPs) with single-particle methods can provide more complete information on particulate populations than bulk measurements.[2] Such measurements could aid in objectives such as source determination of aerosol particulate matter, tracing of particle pollutants in the environment, and understanding past and present earth and climate processes through particulate deposition records.[3-5] In this study, we aim to advance the analysis of Ti-containing particles through the description of a high-throughput single-particle detection and classification strategy. We describe a method to differentiate between naturally occurring Ti-containing (Ti-nat) particles, which are ubiquitous in the environment, and engineered TiO_2 (Ti-eng) particles, which are commercially produced for specific applications.[6-7] The particles studied here have continuous particle size distributions from the nano to sub-micron regimes.

Titanium-containing NPs and µPs can come from natural mineral sources or be produced for industrial/commercial purposes. Primary sources of Ti-nat particles are Ti-containing minerals such as anatase, brookite, ilmenite, perovskite, rutile, titanite, and biotite.[8] Titanium is ninth most abundant element on earth's crust with a crustal abundance of ~0.55%.[9] On the other hand, Ti-eng particles, mostly in the form of TiO_2, are produced on a large scale (8.4 million metric tons globally in 2021)[8] and used in diverse applications primarily for their bright white color, ability to absorb UV radiation, and photocatalytic activity.[10-11] Important classes of products with TiO_2 particles incorporated include paints, plastics, food additives, cosmetics, pharmaceuticals, and solar energy materials.[12-15] Ti-eng particles can ultimately make their way to environmental compartments such as water, soil, and air via sewage spills, waste water treatment plants, urban runoff, and incineration of Ti-particle-containing products.[16-19] The estimated environmental concentrations of Ti-eng particles ranges from ~0.01−16 µg L^{-1} in freshwater.[20-23] Moreover, it has been estimated that up to 50% of all Ti-eng NPs in the environment are contributed by pigment-sized TiO_2 particles, such as the E171 TiO_2 particles investigated in this study.[24]

According to Coll et al., the predicted no effect concentrations, which are the concentrations below which no adverse health effects are expected to occur to an organism,[25] of nano-TiO_2 in fresh water and soil are 15.7 µg L^{-1} and 91.1 mg kg^{-1}, respectively.[21] Increase in concentration of TiO_2 NPs can potentially influence the natural habitat of organisms or animals present in specific environmental compartments.[26-27] For example, one study of the

central nervous system of microglial cells (BV-2) showed that the alteration of cell membrane permeability becomes significant at a concentration of 10 μg mL^{-1} and the death of BV-2 cells at 100 μg mL^{-1}.[28] TiO_2 NPs have also been classified as potential carcinogen with a link to lung cancer in humans.[29] Recently, the European Food Safety Authority (EFSA) in 2021 completed a safety assessment of titanium dioxide (E171) as a food additive and concluded that "a concern for genotoxicity [of TiO_2 particles] could not be ruled out." As a result, EFSA's experts do not consider TiO_2 as a safe food additive.[30]

Many analytical techniques such as atomic force microscopy (AFM), dynamic light spectroscopy (DLS), scanning electron microscopy (SEM), transmission electron microscopy (TEM), inductively coupled plasma optical emission spectroscopy (ICP-OES), and ICP-mass spectrometry (ICP-MS), are used to measure NPs and μPs in environmental samples. AFM and DLS can be used to characterize size distributions, but they do not provide elemental composition information.[31-32] In combination with size-based separation approaches, such as size-exclusion chromatography or field-flow fractionation, ICP-MS can provide multi-element concentration information on size-separated particle populations.[33-35] SEM and TEM have been used to study morphology and size of individual particles down to nanometer scale.[36-38] They also provide elemental composition when coupled with energy dispersive X-ray spectroscopy (EDX); however, the low throughput of these methods limit the detection of low particle number concentrations (PNCs), and is especially challenging for the analysis of analyte NP and μP types against high particle backgrounds. Although automated systems have been developed to employ electron microscopy for NP and μP analysis, long run times and high detection limits are the major limitations.[36,38]

Single-particle ICP-MS (spICP-MS) was first reported in 2003 by Degueldre et al. to analyze colloids of aluminum, titanium, and iron.[39] spICP-MS is an attractive method for the measurement of dilute particle suspensions because it requires minimal sample preparation, is high throughput, and provides simultaneous assessment of element composition, element mass amounts in particles, and PNCs. In spICP-MS, discrete particles are vaporized, atomized, and ionized in the ICP, and produce clouds of ions that—after being extracted into the mass analyzer—have temporal durations of ~200 to 500 μs. In the mass analyzer, the discrete ion clouds are separated according to ions' mass-to-charge (*m/z*) ratios such that element- and isotope-specific transient signals are recorded for each particle. spICP-MS has been used to determine mass and number concentrations of particles ranging in size from 5 nm – 1 μm; however, information regarding elemental composition at single particle level is limited by number of elements that can be simultaneously measured.[38,40-44] By using time-of-flight mass spectrometry (TOFMS), ions across the entire atomic mass range —from ^{6}Li to ^{238}U—can be analyzed quasi-simultaneously with sufficient time resolution to detect particle-produced transient events.[45-47] With spICP-TOFMS, multi-elemental signals from individual particles are recorded as coincident signal spikes at specific *m/z* channels on the signal time trace. Here, we use the terms "single-metal" and "multi-metal" (sm and mm) to refer to particle events measured with either one or with two or more ICP-TOFMS-detectable elements. Some

elements that are commonly present in NPs and µPs, such as carbon, nitrogen, oxygen, sulfur, and fluorine, are not readily detectable at the single-particle level by spICP-TOFMS due to their low masses, high ionization potentials, and/or high natural backgrounds.

Multi-element composition and element/isotope mass ratios recorded from individual particles, can be used to fingerprint and classify engineered and natural particles. Multi-elemental fingerprinting with spICP-TOFMS was first demonstrated by Praetorius et al. to distinguish cerium-containing natural particles from CeO_2 engineered particles.[48] Since then, multi-element fingerprinting by spICP-TOFMS has emerged as a preferred approach to classify NPs and µPs at the single particle level,[16,49-53] although single-particle XRF studies have also been performed.[54] For the characterization of the anthropogenic fraction of Ti-eng particles in environmental samples, most of the existing ICP-MS methods rely on bulk analysis. In these methods, bulk concentration ratios of, for example, Ti:Nb, Ti:Al, Ti:V or Ti:Y are used to indirectly quantify the input of Ti-eng particles, which would elevate each of these ratios with respect to their crustal abundance ratios.[16,19,38,55] Machine learning (ML) models have also been developed to classify and quantify individual Ti-eng and Ti-nat particles in soil samples based on Ti mass amounts and elemental fingerprints.[49,56] These ML approaches require well-characterized training sets from particles whose compositions and size distributions match those expected to be found in environmental samples. Researchers found that these ML models are unable to distinguish some Ti-nat and Ti-eng particle types when Ti-containing NPs that have Ti-mass distributions. In this study, we use spICP-TOFMS to provide particle resolved classification irrespective of the size distribution. We classify and quantify Ti-nat particles from rutile, ilmenite, and biotite minerals and Ti-eng particles from E171 (TiO_2). To test the applicability of our method, we measure Ti-eng spiked into stream water and quantify these particles against Ti-nat particles present in the environmental matrix, as well as other background particles.

Materials and methods

Sample preparation for spICP-TOFMS measurements

Mineral specimens of biotite ($K(Fe^{2+}/Mg)_2(Al/Fe^{3+}/Mg/Ti)([Si/Al/Fe]_2Si_2O_{10})(OH/F)_2$), ilmenite ($FeTiO_3$), and rutile ($TiO_2$) were obtained from the Colorado School of Mines Earth Science Museum. Samples were hand ground in a porcelain mortar and pestle prior to spICP-TOFMS analysis. Neat suspensions of minerals were prepared by dispersing ~5 mg of ground mineral into 15 mL of ultrapure water (18.2 MΩ-cm PURELAB flex, Elga LabWater, UK). Each of these samples were then water-bath sonicated (VWR Ultrasonic Cleaner, VWR, PA, USA) for 10 minutes, vortexed for 30 seconds, and allowed to settle for 10 minutes. Supernatants from these initial suspensions were diluted in ultrapure water containing 5 ng mL^{-1} Cs and spICP-TOFMS analyses were performed to estimate PNCs. Following spICP-TOFMS analyses, the particle suspensions were diluted to achieve stock suspensions with PNCs of ~1×10^6 particles mL^{-1} for each particle type. Subsequent dilutions were made from the stock suspensions with ultrapure water containing 5 ng mL^{-1} dissolved Cs as the diluent.

Food grade titanium dioxide (E171) was purchased from Sigma-Aldrich (Burlington, MA, USA) and used as the representative anthropogenic Ti-eng type. To prepare a neat suspension, ~2 mg of E171 powder was placed in a 2 mL microcentrifuge tube and diluted with 1.5 mL of ultrapure water. The mixture was then vortexed for 30 seconds and ultrasonicated (VialTweeter, Hielscher UP200st, Germany) for 60 seconds (10 seconds on and 5 seconds off) at 100 W. The sonicated sample was centrifuged for 2 min at 4000 rpm using (Mini centrifuge, Costar, USA) and 900 µL of the supernatant liquid was transferred to new 2 mL microcentrifuge tube. The estimated size cutoff from this centrifugation was 400 nm. This initial suspension was diluted in ultrapure water containing 5 ng mL^{-1} dissolved Cs and spICP-TOFMS analysis was performed to estimate PNC and a stock suspension was made with ~1×10^6 particles mL^{-1}. Subsequent dilutions for particle-mixture experiments were made from this stock suspension with ultrapure water containing 5 ng mL^{-1} dissolved Cs as the diluent.

Ti-eng particles were quantified in suspensions with two different background concentrations of Ti-nat particles. The Ti-nat particle suspensions had number concentration ratios of ~7:5:4 (biotite:ilmenite:rutile) and PNCs of about 7,000 mL^{-1} and 45,000 mL^{-1} for the lower-concentration and higher-concentration matrices, respectively. The number ratio of Ti-nat particles in the control mixture sample is arbitrary; all PNCs are within a factor of two. The estimated relative abundances of Ti-bearing minerals in the environment are ~90% ilmenite and 2-10% are rutile.[57] Ti-eng particles were spiked into each Ti-nat particle suspension at a series of PNCs that spanned three orders of magnitude: a table describing sample dilutions for this experiment is provided in the supporting information (Table S1).

Ti-eng and Ti-nat particles were also quantified in suspensions with constant Ti-eng PNC, but variable Ti-nat PNC. These experiments probe the ability of our method to measure Ti-eng particles in variable PNCs of Ti-nat particles. Ti-eng particles were measured at two PNCs: ~4,500 mL^{-1} and ~35,000 mL^{-1}. Ti-nat particles had PNCs spanning two orders of magnitude: from ~440 mL^{-1} to ~90,000 mL^{-1}. Table S2 provides details of the dilutions for this experiment.

Ioway Creek water sample was collected (on March-07-2023) in a 500 mL polypropylene bottle and stored in refrigerator at 4°C. The bottle was thoroughly shaken and 1.5 mL of sample was transferred into 2 mL microcentrifuge tube. The sample was ultrasonicated and centrifuged with the same procedure as for the E171 stock suspension, and 900 µL of the resulting supernatant was transferred to a 4 mL Nalgene bottle. This stream water was then spiked with a E171 particle suspensions to a concentration of 2220 µg L^{-1} Ti, which is an arbitrary concentration based on the concentration of Ti in the E171 stock suspension, and diluted either 200X or 1000X with 5 ng mL^{-1} Cs water. These spiked and diluted stream water samples were then serially diluted with 200X or 1000X diluted stream water + 5 ng mL^{-1} Cs before spICP-TOFMS measurements. This dilution procedure maintains constant stream particle background while the concentration of Ti-eng particles changes. The expected Ti concentrations of spiked Ti-eng particles in stream water ranged from 11 to 2220 µg L^{-1} Ti and are provided in Table S12.

Preparation of microdroplet calibration solution

A multi-element calibration solution was prepared for online microdroplet experiments using single-element standards (High-Purity Standards, SC, USA). The elements used were Mg, Al, Ti, V, Mn, Fe, Cu, Zn, Y, Zr, Nb, Cs La, Ce, and Ta; concentrations for online microdroplet calibration are provided in Table S3. All dilutions were prepared gravimetrically (ML204T/A00, Mettler-Toledo, Greifensee, Switzerland) using 2% a sub-boiled trace metal grade nitric acid (Fisher Scientific, Fair Lawn, NJ, USA) as the diluent. Cesium (Cs) was used as the plasma uptake standard for online microdroplet calibration.

spICP-TOFMS measurements and data processing

An icpTOF-S2 instrument (TOFWERK AG, Thun, Switzerland) was used for all measurements; instrument operating parameters are given in Table S4. Calibrant microdroplets were introduced via a dual-sample introduction setup and element masses per particle and PNCs were determined using online microdroplet calibration, as described elsewhere.[58-59]

All data were collected with TofDAQ Recorder (Tofwerk AG, Thun, Switzerland) and then processed with our in-house "TOF Single-Particle Investigator" (TOF-SPI) program, written in LabVIEW (LabVIEW 2018, National Instruments Corp., TX, USA). TOF-SPI is a batch analysis program designed for online microdroplet calibration. The program is used to calculate element background signals and single-particle critical values, determine absolute element sensitivities, background subtract data, correct split-particle events,[60] quantify element masses in single particles, and determine PNCs.

The single-particle critical value ($L_{C,sp}$) is the detection threshold used to separate particle-derived signals from steady-state dissolved element background signals and is calculated as a one-sided detection decision with element-specific false-positive rates between 1×10^{-3} and 1×10^{-7}. The calculation of $L_{c,sp}$ is done in a similar manner as recommended by the IUPAC;[61] however, we use compound-Poisson statistics to calculate $L_{c,sp}$ because the dispersion of low-count icpTOF data is not adequately described by Normal or Poisson distributions.[62-63] $L_{c,sp}$ can be converted to a critical mass ($X_{c,sp}^{mass}$) based on a calibration factor (absolute sensitivity) and a critical diameter ($X_{c,sp}^{diameter}$) by assuming a particle geometry, stoichiometry, and density.

In Table S3, we report the nuclides used for quantification of elements in detected particle events, and typical absolute sensitivities and critical mass values. For some recorded Ti-particle events, the signal recorded for $^{48}Ti^{+}$ exceeded the dynamic range of the microchannel plate detector used in the icpTOF instrument. On the icpTOF instrument, the linear dynamic range per *m/z* channel is around 1-20,000 counts per particle event; above 20,000 counts, the signal at a given *m/z* saturates.[64] To overcome these saturation effects and extend the measurement's linear dynamic range, we used $^{48}Ti^{+}$ (natural abundance = 73.7%) to quantify Ti in particles that have signal of $^{48}Ti^{+}$ < 1500 counts and ^{46}Ti (natural abundance = 8.3%) for particle events with $^{48}Ti^{+}$ signal > 1500 counts. At 1500 counts of $^{48}Ti^{+}$, signals from both ^{48}Ti and ^{46}Ti are within their linear ranges. With this approach, Ti in particles can be quantified

from the critical mass (80 ag) up to ~500,000 ag. Details of the performance of this multi-isotope calibration strategy are provided in the Fig. S8.

Classification of individual particle events as Ti-eng, Ti-nat (i.e. rutile, ilmenite, or biotite), unclassified single-metal particles (unc. sm), and unclassified multi-metal particles (unc. mm) was achieved using custom-written Streamlit webApp (version 1.7.0) based on Python language (version 3.9) using Pycharm (Community Edition 2021.3.3) as an integrated development environment (IED). The source codes for our Streamlit webApp are available on GitHub (https://github.com/TOFMS-GG-Group). The classification scheme is discussed below.

Results and discussion

Element compositions of the Ti particles

To ascertain the compositions of Ti-nat and Ti-eng particles at the single particle level, we analyzed neat suspensions of each particle type by spICP-TOFMS. We found that each Ti-nat type has a unique elemental composition compared to that of Ti-eng particles. Ti-eng particles are "pure" at the sensitivity level of the ICP-TOFMS instrument: the only ICP-MS-detectable element they contain is titanium. The unique multi-metal signatures of the Ti-nat particles enable discrimination between each other and the Ti-eng particles. In Fig. 1, we provide correlograms of element masses in Ti-containing single-particles from the three Ti-nat particle types. Heat maps of element mass per particle (Fig. S1), signal time traces (Fig. S2), and representative mass spectra (Fig. S3) also show the unique elemental compositions and element ratios of each type of Ti particle type.

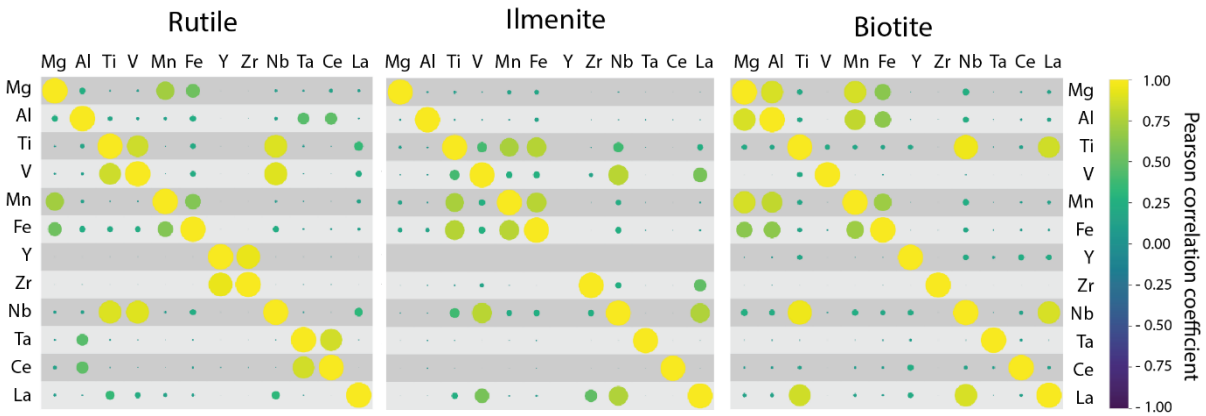

Figure 1. Correlograms of element masses in natural particle types; all particles that have measurable amounts of Ti are included in the correlogram. The correlograms are generated using Streamlit webapp based on Pearson correlation coefficient, which is the ratio between covariance of two variables and product of their standard deviations.

All the Ti-nat particles contain Ti as a major element (>1% mass fraction), though this mass fraction varies from 57% to 1.5% from rutile to biotite. The only element well correlated with Ti in all the particle types is Nb, but the Ti:Nb mass ratio is different between the particle types (see Fig. S4). In rutile particles, Ti is the ICP-MS detectable element with the largest mass fraction and the average mass ratio of Ti:Nb is ~1000:1. Associated elements in rutile particles include Al, V, Fe, La and Ta. In ilmenite particles, Fe and Ti are the ICP-MS detectable elements

with the largest mass fractions and are highly correlated (see Fig. S5) with an Fe:Ti mass ratio that converges to ~1:1. The average Ti:Nb ratio in the ilmenite particles is 150:1 and other associated elements include Mg, Al, V, Mn, and La. In biotite particles, Al and Fe are the most abundant ICP-MS detectable elements, followed by Mg, Ti, and Mn. Fe and Al are each well correlated with Ti in the individual biotite particles; elemental mass ratios converge to 16:1 and 7:1 for Fe:Ti and Al:Ti, respectively (see Fig. S5). The average Ti:Nb mass ratio in biotite is 25:1 and other associated elements include La and Ta. In Table S5, we provide the average mass fractions of all elements recorded in each particle type and in Table S6 we provide the bulk mass fractions from digested particle samples analyzed by conventional ICP-MS. The bulk mass fractions and element mass ratios for all particle types match well with those recorded from individual particles with the exception of Ti:Nb in the ilmenite particles, which have a Ti:Nb mass ratio of 58:1 in the bulk digest and an average mass ratio of 122 in the particles. The Ti:Nb mass ratio is more scattered in ilmenite particles compared to biotite and rutile particles, which indicates that real variability in mass fractions of Nb are the likely cause of the discrepancy between bulk and particle Ti:Nb mass ratios.

As seen by the correlograms (Fig. 1), element heatmaps (Fig. S1), bulk characterization (Tables S5 and S6), and mass correlations (Fig. S4 and S5), the four Ti particle types examined here have clear differences in elemental composition. However, at the single-particle level, differentiating between the particle types is complicated by the size of individual particles. For smaller particles, the most abundant elements may be detectable, while lower abundance elements remain undetected, i.e. below element-specific $L_{C,sp}$ values. In addition, at single particle level, differentiation of the particles based only on their elemental compositions is challenging because many particles have similar compositions and elemental ratios show scatter due to Poisson statistics.

In Fig. 2, we plot the mass distributions of Ti particles recorded with single-metal (sm), i.e. Ti-only, and multi-metal (mm) compositions from each particle type and the stream water sample. As seen, Ti-eng particles are always detected as sm; the presence of a secondary element cannot be used to identify the Ti-eng particles. Even though all the Ti-nat particles have some portion of events that are mm, sm-Ti events are also recorded and so an approach must be devised to differentiate the sm-Ti events from Ti-eng vs. Ti-nat sources. The Ti-nat particle type with the most recorded Ti-sm events is rutile. Some rutile particles are recorded as Ti-sm because Ti is the major ICP-MS detectable element in these particles, and so can be detected from small particles that have minor element amounts below their $\mathrm{X}_{\mathrm{c,sp}}^{\mathrm{mass}}$ values. However, as seen in Fig. 2, the Ti mass distributions of sm-Ti signatures from Ti-eng and rutile particles only partially overlap. As rutile particles get larger (i.e. Ti mass goes up) the probability of measuring a mm signature in the particles increases and so these larger rutile particles can be distinguished from Ti-eng particles based on their recorded multi-metal compositions. Ti-sm particle signatures are observed from the ilmenite and stream water samples; however, for ilmenite the Ti mass in these particles is less than that recorded from the rutile sample and consequently it does not significantly interfere with the identification of sm Ti-eng particles. For both the ilmenite and biotite, sm-Ti particle events are less often

recorded because Ti is less abundant than other ICP-MS detectable elements (Al and Fe biotite) or detected with less sensitivity than other major elements (Fe in ilmenite).

In Table 1, we report the average mass of Ti per particle, the equivalent spherical diameter, and the interquartile size range of each NP type measured. Particle masses are estimated based on known stoichiometry of the particle (i.e., as oxides or silicates) and diameters are calculated assuming spherical shape and mineral densities.[65-67] In Figure S6, we provide particle diameter histograms of the E171, rutile, ilmenite, and biotite particles. All these particles have similar size distributions, with between 30-70% of particles in the nano-regime (diameter < 100 nm), and the remaining particles in the sub-micron regime with more than 95% of particles with diameters less than 500 nm.

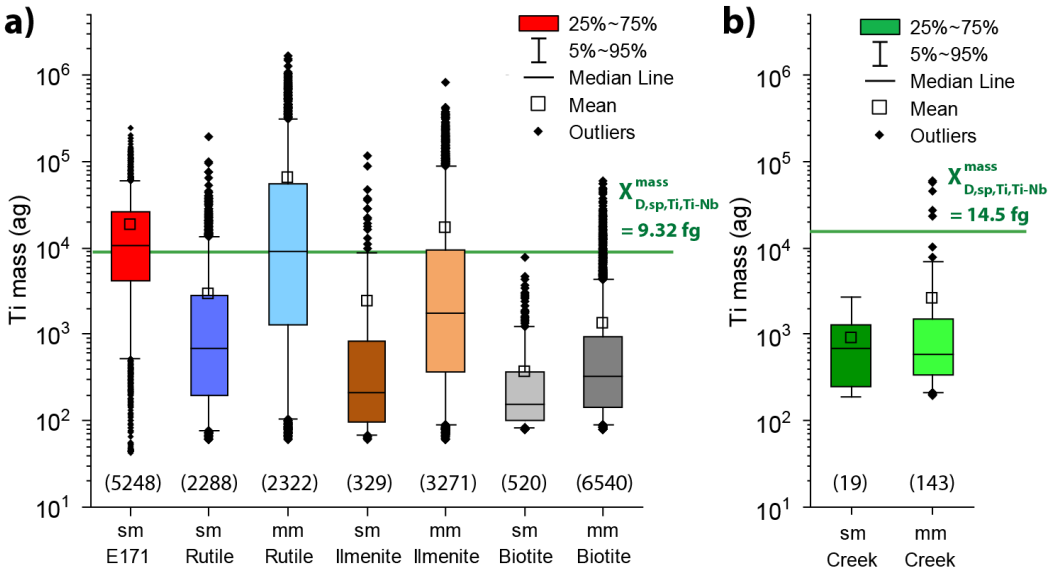

Figure 2. a) Ti mass distribution in different type of Ti-eng and Ti-nat NPs and µPs found in both Ti single metal (sm) and multi-metal (mm) particles. The mass of Ti in the particles spans more than four orders of magnitude and there is substantial overlap in the Ti mass distributions of sm-Ti particles from E171 and rutile. $X^{mass}_{D,sp,Ti,Ti-Nb}$ is the particle-type detection limit; above this threshold, sm-Ti particles are considered to be from E171; however, below this threshold sm-Ti particles are unclassified because they could be Ti-eng or Ti-nat rutile particles. B) Ti mass distributions from Ti-sm and Ti-mm particles measured in the Ioway Creek sample. $X^{mass}_{D,sp,Ti,Ti-Nb}$ is slightly different for this sample because sensitivity of Ti and Nb are different. Numbers of particles recorded for the detected sm-Ti and mm-Ti particle events are provide in parentheses; these values are obtained from individual measurements.

Table 1. Average particle size and average mass of all E171, and rutile, ilmenite, and biotite particles. The average values and standard deviations are based on triplicate measurements.

Particle type	Density (g/cm^3)	Average diameter (nm)	Interquartile size range (nm)	Average mass of Ti in NP (fg)
E171	4.23	177 ± 2	105 ± 2	20 ± 1
Rutile	4.23	152 ± 7	133 ± 3	30 ± 4
Ilmenite	4.7	159 ± 3	134 ± 4	15 ± 1
Biotite	3.1	203 ± 1	126 ± 4	1.2 ± 0.1

Particle-Type Detection Limit Filtering to Differentiate Ti-eng from Ti-nat Rutile Particles

To differentiate between sm Ti-eng particles and those that come from rutile, we define a particle-type detection limit. Particle-type detection limits were first reported by Szakas et al.[68] and describe the minimum amount of signal from a major element (i) that is required to also measure a minor element (j) at a certain significance level. These particle-type detection limits ($L_{D,sp,i,i-j}$) can be developed for any particle types that have major-minor element pairs with known mass fractions. $L_{D,sp,i,i-j}$ is defined in equation 1, where $L_{D,sp,j}$ is the detection limit for the minor element j and $R_{cts,i:j}$ is the signal ratio in counts of i:j in a given particle type. The detection limit of element j is defined in equation 2 and is calculated using Poisson-Normal statistics as a two-sided detection limit that depends on user defined false-positive (α) and false-negative (β) rates.[61,69] For single-particle analysis, the lower detection bound (α) is defined by the critical value ($L_{C,sp,j}$), while the false-negative rate describes the fraction of the measured distribution that is above $L_{C,sp,j}$ and is calculated using a z-score ($z_{1-\beta}$). The value of β is commonly set to 5%, so that 95% of the measured signal is above $L_{C,sp,j}$.

In equation 3, we present the particle-type detection limit for measuring a major element (Ti) with a minor element (Nb) at a false negative rate of 5% ($z_{1-\beta} = 1.64$). To determine the $L_{D,sp,Ti,Ti-Nb}$ for a given particle type, we must set the Ti:Nb signal ratio. This count ratio can be calculated based on a known elemental mass ratio of the major and minor elements and the spICP-TOFMS sensitivities ($S_{drop,Ti}$ and $S_{drop,Nb}$) for each element as determined by online microdroplet calibration, as seen in equation 4. In equation 5, the particle-type detection limit is expressed in terms of the mass of Ti by dividing $L_{D,sp,Ti,Ti-Nb}$ by the sensitivity for titanium ($S_{drop,Ti}$).

$$L_{D,sp,i,i-j} = L_{D,sp,j} \times R_{cts,i:j} \quad (1)$$

$$L_{D,sp,j} = \left(\frac{z_{1-\beta} + \sqrt{(-z_{1-\beta})^2 + 4L_{C,sp,j}}}{2} \right)^2 \quad (2)$$

$$L_{D,sp,Ti,Ti-Nb} = \left(\frac{1.64 + \sqrt{(-1.64)^2 + 4L_{C,sp,Nb}}}{2} \right)^2 \times R_{cts,Ti:Nb} \quad (3)$$

$$R_{cts,Ti:Nb} = R_{mass,Ti:Nb} \times \frac{S_{drop,Ti}}{S_{drop,Nb}} \quad (4)$$

$$X^{mass}_{D,sp,Ti,Ti-Nb} = \frac{L_{D,sp,Ti,Ti-Nb}}{S_{drop,Ti}} \quad (5)$$

$L_{D,sp,Ti,Ti-Nb}$ values can be established for any Ti particle type with a known Ti:Nb mass ratio. In Fig. S4, we plot the quantified mass-amounts of Nb and Ti recorded in individual particles from the Ti-nat particle samples. In all the Ti-nat particles, Ti and Nb are correlated, though the ratio is different for each particle type, as previously discussed. To limit false classification of Ti-nat particles as Ti-eng , we established $L_{D,sp,Ti,Ti-Nb}$ using the average crustal mass ratio

of Ti:Nb, i.e. 300:1 Ti:Nb.[9] $L_{D,sp,Ti,Ti-Nb}$ sets the minimum signal of Ti required to detect Nb (at 95% confidence) in a Ti-particle with Ti:Nb at the crustal ratio. If a sm-Ti particle is detected with Ti signal above $L_{D,sp,Ti,Ti-Nb}$, then we consider that particle event to be Ti-eng. However, if a sm-Ti particle event is recorded with titanium signal below $L_{D,sp,Ti,Ti-Nb}$, then the particle is unclassified (unc. sm). We use the crustal ratio of Ti:Nb to classify sm-Ti particles because this threshold provides acceptable levels of false-positive Ti-eng classifications (< 5%) and true-positive Ti-eng classification (>50%). In Figure S7, we present the true and false positive Ti-eng classification percentages as a function of the Ti:Nb mass ratio used to define the particle-type detection limit, $L_{D,sp,Ti,Ti-Nb}$. While particle-type detection limits can be expressed in terms of mass of Ti, the detection limits are fundamentally calculated in the signal domain because that is the domain of Poisson statistics. $L_{D,sp,Ti,Ti-Nb}$ values are calculated for each analyzed sample depending on experimental parameters, including $L_{C,sp,Nb}$, $S_{drop,Ti}$, and $S_{drop,Nb}$. Here, the average $L_{D,sp,Ti,Ti-Nb}$ is 635 counts and the $X^{mass}_{D,sp,Ti,Ti-Nb}$ is 9.32 fg, which translates to a diameter of 211 nm for TiO_2.

Decision tree for the classification of Ti particles

In Figure 3, we provide the decision tree for the classification of Ti-containing particles as Ti-eng, Ti-nat, and the different mineral types of Ti-nat particles. In addition to classification of sm-Ti particles as Ti-eng based on $L_{D,sp,Ti,Ti-Nb}$, particles with mm-Ti signatures are classified based on unique element associations and/or elemental mass ratios. Specifically, we find that the detection of Fe, Mn, Nb, and La—along with Ti—are the most useful for differentiating the Ti-nat particle types. Ti and Fe are well correlated in both the ilmenite and biotite samples and have significantly different Fe:Ti mass ratios of 1:1 and 16:1, respectively. Based on Fe:Ti mass ratio thresholds, Ti:Nb mass ratio thresholds, and presence of Mn and La, the three Ti-nat particle can be classified (see Fig. 3 for details). Some portion of Ti-containing particles with sm and mm signatures cannot be successfully classified, and so are unclassified (unc.). Unclassified sm-Ti particles (unc. sm-Ti) are determined based on the particle-type detection limits as described above. Unclassified mm-Ti particles (unc. mm-Ti) can be classified as Ti-nat particles, but can't be reliably assigned to a mineral type. The threshold ranges of element mass ratios for Ti-nat particle type assignment boundaries are determined empirically such that >75% of particles of a given type have mass ratios that fall within a given range. Natural variability of mass ratios, particle size distributions, and detection statistics preclude the possibility of 100% accurate particle classifications.

Accuracy of classification scheme

To determine the accuracy of our decision tree classification scheme, particles were classified from neat suspensions of each particle type and then from a mixture of Ti-nat particles. Figure 4a-d shows true and false classification percentages of each particle type in neat suspensions and Figure 4e shows the Ti-nat particle mixture sample; all classification percentages are in terms of particle numbers. Overall, our classification approach minimizes false-positive particle-type assignments, which were less than 5% for all particle types. Some particles, such as E171 and rutile, produced many false negative unc. sm-Ti classifications. We expect many

false-negative results because small NPs and µPs—which are the ones most often labeled as unclassified—have fewer detectable elements to distinguish particle types. While Ti-eng particles with diameters < 211 nm remain unclassified, small Ti-nat particles in the nano-regime can be accurately classified based on their unique multi-element fingerprint.

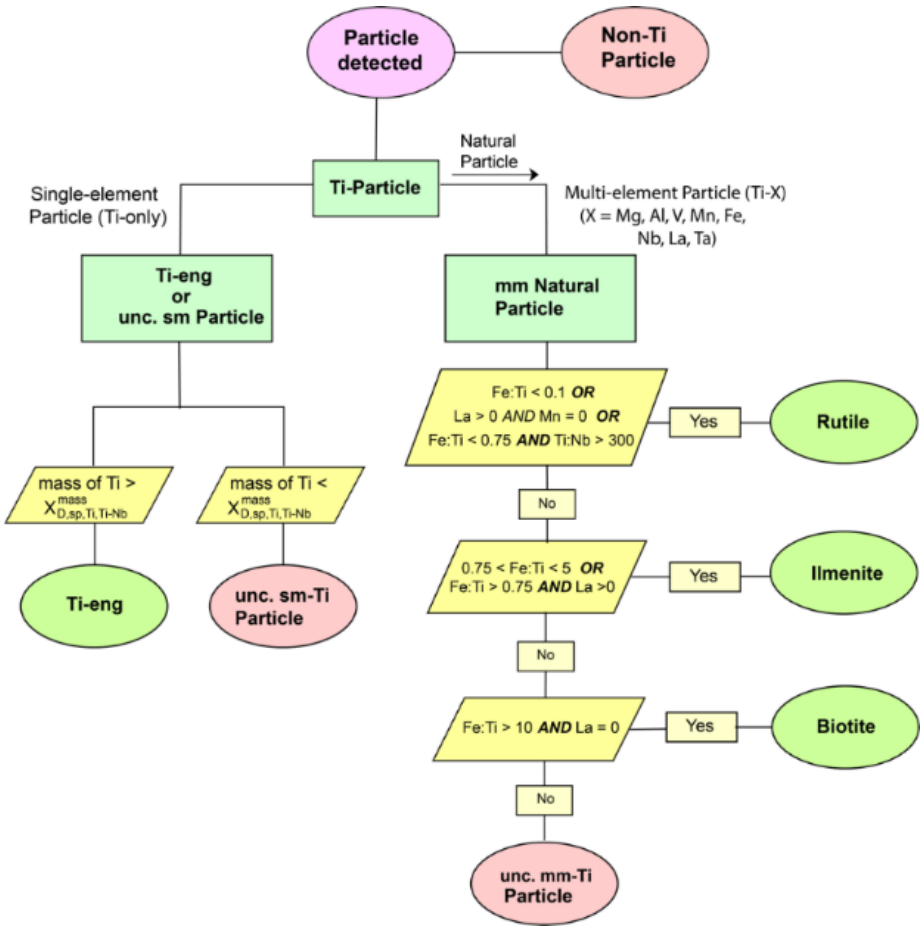

Figure 3. Decision tree for classification of Ti-containing NPs and µPs. All element ratios are in terms of mass.

Distinguishing between E171 and rutile particles is, by far, the most challenging, and leads to the most unclassified Ti-sm particles and the most false-positive Ti-eng classifications. From the neat suspension of E171, 54.6% of the particles are correctly classified with no false positive Ti-nat classifications, but 45.2% are reported as unc. sm-Ti because they have masses below $X^{mass}_{D,sp,Ti,Ti-Nb}$ (~9.32 fg of Ti). In the case of rutile, 32.3% of particles are correctly classified with 4.4% false-positive Ti-eng classification and 45.7% unc. sm-Ti. While many rutile particles are unclassified, the unclassified number fraction is greatly affected by the particle size distribution; as seen in Table 1 and in Figure S6, the rutile particles are, on average, the smallest Ti-nat particles tested, with ~70% of particles in the nano-regime (diameter < 100 nm).

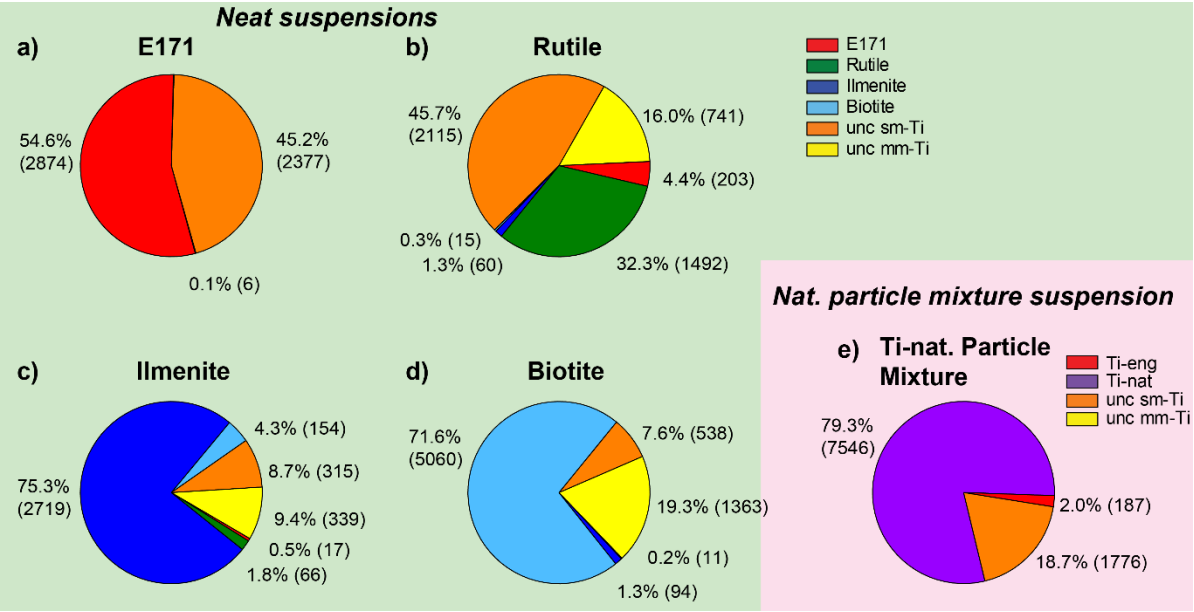

Figure 4. a-d) Pie charts showing true and false-positive classifications of each type of Ti-particles from neat suspensions. Classification decision tree is provided in Figure 3. Percentages are calculated in terms of particle number (absolute number reported in parentheses). e) Results from the binary classification (Ti-eng or Ti-nat) of a mixture of only Ti-nat particles. In this sample, all particles classified as Ti-eng are false positives. The classified particle numbers and classification percentage provided in the figure 4 are from an individual measurement. The average classified particle numbers and classification percentage from triplicate measurements are given in Tables S10 and S11.

Ilmenite and biotite are more straightforward to separate from the Ti-eng particles because these particles have other ICP-MS detectable elements with equal or greater abundance than Ti. From ilmenite particles, only 0.5% are falsely classified as Ti-eng and 75.3% of particles are correctly classified. In the case of biotite, no false-positive Ti-eng particles are found and 71.6% of particles are correctly classified. Ilmenite and biotite are primarily distinguished based on Fe:Ti ratios. Even though Mg, Al, and Mn are present and correlated in the biotite particles, they cannot be used for biotite classification because these elements are not correlated—though may be present—in the other particle types. For example, it would be likely to measure an ilmenite particle with the similar Al:Ti ratio as that found in biotite particles and so produce an inconclusive classification (see Figure S5b). On the other hand, as shown in Figure S5a, good correlation between Fe and Ti in both the ilmenite and biotite particles allows for accurate mineral classification based on the Fe:Ti ratio.

In a mixture of all the Ti-nat particle types (PNCs of biotite:ilmenite:rutile = 7:5:4), 79.3% of particles are correctly classified as Ti-nat and only 2.0% are falsely classified as Ti-eng. The binary classification of Ti-eng and Ti-nat results in fewer unclassified particles because all mm-Ti particles are classified as natural and no distinction between the mineral types is attempted. Because ilmenite produces fewer false-positive Ti-eng classifications than rutile, false-positive Ti-eng classifications in environmental samples could occur less frequently than that found in our control mixture. However, this will depend on a sample's mineralogy and particle-size distributions. Moreover, the classification of particles will also depend on the

geological location and its polymorphic state. Under certain hydrothermal conditions, polymorphs of rutile (TiO_2), such as anatase and brookite, can also be produced. Although the major elemental composition is same in the polymorphs, there could be some difference in composition and content of minor elements.[70-73]

In Fig. 5, we plot Ti:Nb mass ratios as a function of Ti mass in particles from neat suspensions and in classified particles from the Ti-nat particle mixture. Apart from rutile, the Ti-nat types are not classified based on presence or mass ratio of Nb. Nonetheless, Nb shows correlation with Ti in all the Ti-nat particle types. After classification, the general shapes of the Ti:Nb distributions for each of the classified Ti-nat types matches that recorded from the neat suspensions, and thus confirms mineral type classification accuracy. This result illustrates the potential of spICP-TOFMS for particle-by-particle mineralogy of Ti-rich particles which could, for example, be useful in source apportionment studies of mineral dust aerosols.[74-75] Bulk Ti:Nb ratios from digested particle suspensions are 22, 59, and 1060 for biotite, ilmenite, and rutile, respectively (see Table S8). The lower Ti:Nb mass ratio recorded in the bulk for ilmenite could be due to true heterogeneity in the mass fraction of Ti in the particles, and is also evident in the scatter plots in Figure 5.

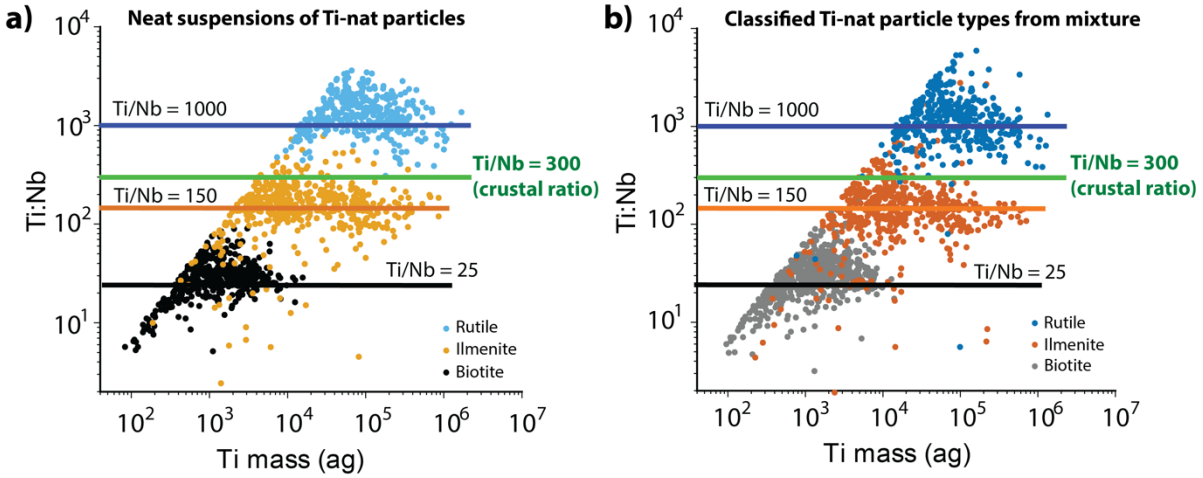

Figure 5. Titanium-to-niobium (Ti:Nb) mass ratio plotted against Ti mass for each type of Ti-nat particle. a) Ratios from particles with known composition from neat suspensions of each Ti-nat particle. b) Ti:Nb ratios found in classified particles from a mixture of mineral particles. Good match between (a) and (b) indicates accurate Ti-nat particle-type classification.

Quantification of engineered and natural particles

Quantification of anthropogenic NPs and µPs in environmental samples can be challenging due to low concentrations of anthropogenic particles compared to the natural background.[18] To further validate our particle classification scheme, we created mixtures of E171 and Ti-nat particles with variable number concentrations. This experimental design was used to build and validate our particle classification scheme. In Fig. 6, we present results in which Ti-eng particles are detected, classified, and quantified across PNCs spanning three orders of magnitude in two different Ti-nat backgrounds (with ~7000 and ~45,000 Ti-nat particles mL^{-}

[1]). In the lower Ti-nat PNC sample (Fig. 6a), detected particle number ratios of Ti-eng to Ti-nat ranged from 1:14 to 20:1. In the higher Ti-nat PNC sample (Fig. 6b), detected particle number ratios ranged from 1:62 to 3:1 (Ti-eng:Ti-nat). In Figure S9, we provide results for the quantification of a constant amounts of Ti-eng particles against variable Ti-nat PNCs.

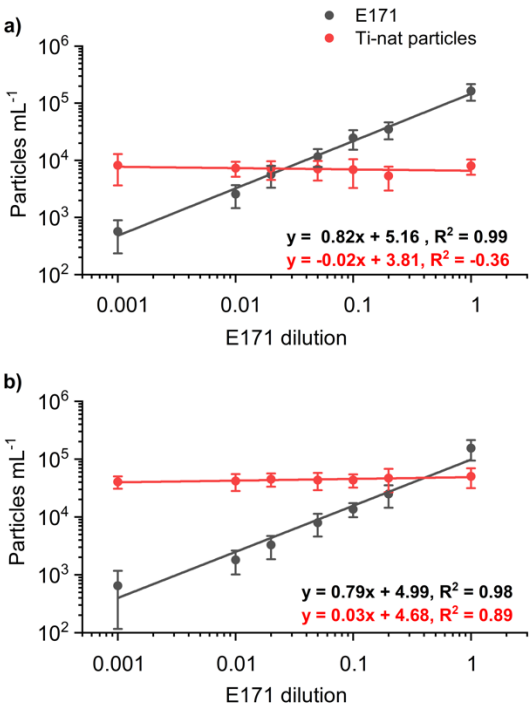

Figure 6. Quantitative analysis of Ti-eng particles in samples with lower (a) and higher (b) PNCs of Ti-nat particles. A linear response can be seen with increasing concentrations Ti-eng particles. Average values and error bars are based on triplicate measurements. E171 dilution refers to the dilution of E171 stock suspension.

In Fig. 6a and 6b, the slope of the number of classified Ti-eng particles is ~0.8. A slope of 1 on a log-log plot indicates direct proportionality, whereas the found slope of less than 1 indicates that slightly fewer particles are classified as Ti-eng particle than would be predicted by the increase in concentration of the particles. When the PNC increases by an order of magnitude (10x), the number of Ti-eng particles detected only increases 8x. A cause for this non-linearity is the presence of a small constant number of rutile particles classified as Ti-eng; this offset is apparent in Fig. 6b, in which the lowest concentration of Ti-eng is elevated. At a low PNC, false-positive Ti-eng classification can cause a relatively large contribution to the total number of particles recorded. Based on the Ti-eng false-positive rate of 2.0% found in Fig. 4e, a Ti-nat PNC of 45,000 particles mL^{-1} would provide a constant Ti-eng false-positive background of ~900 particles mL^{-1}, which is similar to the PNC observed at the lowest concentration of Ti-eng particles in Fig. 6b. One way to limit this false classification rate is to increase the particle-type detection limit ($L_{D,sp,Ti,Ti-Nb}$) by either increasing the expected Ti:Nb mass ratio (see Fig S7) or decreasing the allowable false-negative rate (β value). However, both of these measures would also cause fewer true Ti-eng particles to be classified. With our current classification strategy, we demonstrate that Ti-eng particles can be detected at a number concentration 60-times lower than that of Ti-nat particles.

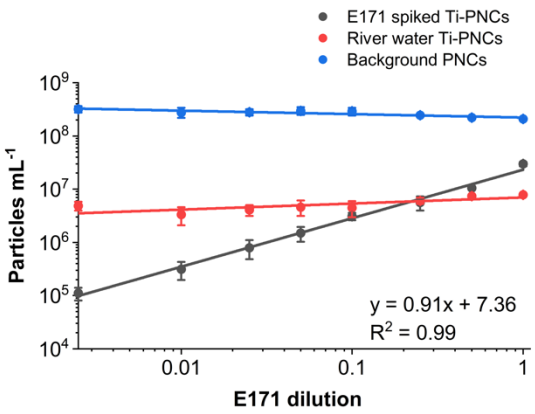

Figure 7. Quantitative analysis of spiked E171 particles in stream water. Average values and error bars are dilution-corrected and based on triplicate measurements. E171 dilution refers to the dilution of E171 stock suspension.

To test our Ti-particle classification strategy in a real-world situation, we collected natural stream water from Ioway Creek (Ames, IA on March 7, 2023) and then performed spike and recovery studies of E171 particles spiked into the stream sample. This sample was found to to have no (below detectable amounts) Ti-eng particle concentrations and so is considered "pristine" and to only contain Ti-nat particle for our analyses. The stream water sample is much more complex than our neat control suspensions of Ti-nat particles. Importantly, most of the particles in the stream water do *not* contain titanium. In Table S9, we provide details of the background particles recorded. As detected by spICP-TOFMS, 96% of the detected particles in the stream sample are composed of either Fe or Al, and the most abundant particle types by number are sm-Fe (46%) and mm-AlFe (42%). Titanium is detected in only ~2% of particles events and most of the Ti particles are associated with Fe (88%); only 14% of the Ti-particles are sm-Ti. Due to the high background of Fe-rich particles in the stream water, the major challenge in detecting Ti-eng particles in this matrix is avoiding false coincidence of Ti-eng particles with Fe and Al particles; this is accomplished through dilution of the samples.[58] For spike and recovery studies, E171 particles were spiked into the stream water at an initial concentration of 2215 µg L^{-1} Ti-eng particles, were well mixed, and then diluted either 200 or 1000 times to reduce the background PNCs. These 200x and 1000x spiked stream water samples were then further diluted with either 200x or 1000x diluted stream water to simulate variable Ti-eng PNCs in a constant stream matrix. After spICP-TOFMS analysis, particle signals were classified according to our established rules (see Fig. 3) with $X^{mass}_{D,sp,Ti,Ti-Nb} = 14.5$ fg; the particle-type detection limit here is different than that found for the neat suspensions because $X^{mass}_{D,sp,Ti,Ti-Nb}$ depends on the absolute sensitivity and critical value from each measurement. Results for the classification of Ti-nat and spiked Ti-eng particles in the stream water are provided in Fig.7 and Fig. S10. In Table S12 and Fig. S11, we provide the recovery of the Ti-eng particles in terms of mass concentration (µg L^{-1}). In addition, we also performed bulk analysis of stream water and found that magnesium has significantly higher concentration (~27 mg L^{-1}) than other elements. The total concentration of Ti was found to be 143 ± 43 µg L^{-1}, which is in the range of the total concentration of Ti found

in rivers in South Carolina.[76] The bulk elemental concentration of stream water is provided on Table S13.

Overall, the mass concentration recovery of E171 particles was greater than 50% in all samples and the Ti-eng particles could be measured at a range of PNCs spanning almost three orders of magnitude. The Ti-eng particles were recorded at a PNC 44 times below that of the Ti-nat background in the Ioway Creek water and 2850 times below the total PNC (including non-Ti particles) found in the stream sample. At the lowest spiked level, Ti-eng particles were measured at a mass concentration of 0.04 μg L^{-1}, which corresponds to a concentration of 7.4 μg L^{-1} in the undiluted stream water. These concentrations are in the range of predicted environmental concentrations and predicted no-effect concentrations for TiO_2 NPs.[21,23] The biggest challenge to detecting Ti-eng at environmentally relevant concentrations by spICP-TOFMS is the high background of non-Ti particles rather than interference with Ti-nat particles.

Environmental implication

This study is first to report the particle-resolved classification of Ti-nat NPs and μPs of Ti-bearing minerals (biotite, ilmenite and rutile) and engineered titanium dioxide (E171) via spICP-TOFMS and multi-element fingerprints. For this classification, we developed a decision tree strategy that allows for separation of particle types based on particle-type detection limits and element mass ratios in each particle. The approach allows for correct classification of 32%, 75%, and 72% of rutile, ilmenite, and biotite particles and 55% of E171 particles. Importantly, our classification strategy emphasizes low false-positive classification rates: false classification of Ti-nat as another type of Ti-nat or Ti-eng is below 5% in all cases. Minimization and control of false-positive Ti-eng classifications is especially important for the analysis of environmental samples which may have low PNCs of Ti-eng particles and can have variable PNCs of Ti-nat particles. Unlike previous approaches,[49,56] our Ti-eng particle classification does not depend on Ti particle size as a distinguishing characteristic. Instead, classification of Ti-eng particles is based on the presence *or absence* of secondary elements and the predicted mass fraction of these elements in Ti-nat particles. With this approach, TiO_2 particles can be classified in the presence of Ti-nat particles with similar Ti mass distributions, which would be expected in real samples. In our studies, TiO_2 particles with diameters of ~210 nm can be classified, though this critical size for particle classification depends on sensitivities and dissolved background concentrations of elements used to calculate particle-type detection limits, i.e. Ti and Nb. Quantification of anthropogenic submicron TiO_2 in the environment is important to assessing environmental anthropogenic Ti particle concentrations; it has been estimated up to 50% of all nano-sized (<100 nm diameter) TiO_2 particles originate from pigment-sized (i.e. sub-micron) TiO_2 particles.[24]

Through the analysis of controlled mixtures of Ti-nat and Ti-eng particles and Ti-eng particles spiked into a local stream (Ioway Creek, Ames IA), we demonstrated that Ti-eng particles can

be classified and detected at (or near) environmentally relevant mass concentrations. In particular, in the Ioway Creek study, Ti-eng particles can be quantified down to a mass concentration of 0.04 μg L^{-1}, which is within the predicted environmental concentration range for TiO_2 NPs.[21,23] However, detection at this low mass concentration is only possible if the natural sample has relatively low PNCs of all inorganic NP and μPs because high background PNCs require dilution before spICP-TOFMS to avoid particle coincidence during detection. Good linearity of classified Ti-eng PNCs are demonstrated across three orders of magnitude and Ti-eng particles can be measured at PNCs 44-times lower than that of Ti-nat particles in real samples.

In previous research, anthropogenic TiO_2 NP concentration has been estimated based on the comparison of bulk Ti:Nb mass ratios in digested urban water samples and natural background samples.[16,50] In the Ti-nat samples we analyzed, we found that the mass ratio of Ti:Nb is highly mineral dependent. At the single-particle level, biotite has a Ti:Nb mass ratio at ~25:1, ilmenite has ratio of ~150:1, and rutile has a ratio of ~1000:1. None of the mineral types have Ti:Nb mass ratios that match the crustal Ti:Nb ratio of ~300:1.[9] These results suggest that use of the enhancement or depletion of bulk Ti:Nb ratios compared to the crustal ratio to estimate the concentration of Ti-eng particles would be heavily influenced by natural mineral distributions in a given sample. On the other hand, particle-resolved classification of Ti-eng particles based on spICP-TOFMS could provide a more robust quantification of anthropogenic Ti-particle inputs and also would allow detection of Ti-eng particles in the presence of NPs and μPs with high mass fractions of Nb.

Overall, the spICP-TOFMS analysis scheme developed here shows promise for classification of trace concentrations of Ti-eng particles in environmental samples independent of baseline Ti:Nb concentration ratios or Ti particle size distributions. In the future, we will expand this work to characterize and quantify Ti-eng and Ti-nat particles in other environmental samples such as soils, sludges, and urban runoffs. In addition, consideration of other anthropogenic Ti-rich particles types, such as nanocomposites from sunscreens, or Ti-nat particles from, e.g. anatase, brookite, or titanomagnetite, would enable us to expand and refine the classification approach.

ASSOCIATED CONTENT

Supporting information

Dilution schemes for quantification of E171 and Ti-nat particles; ICP-TOFMS instrument parameters and online microdroplent calibration parameters; average mass fractions of elements in each particle type; bulk mass fractions of elements in each mineral type as well as stream water from total digestion with ICP-TOFMS anlaysis; Fe:Ti and Ti:Nb mass ratios from bulk and single particle analysis; Ti-mineral and stream water digestion procedure; tabulated results of spICP-TOFMS analysis of stream water; average classified particle numbers, classification percentages and standard deviations of each particle types from neat particle suspensions and mixed Ti-nat sample; spike and recovery results spICP-TOFMS

analysis of E171 particles in stream water; heat maps showing elemental compositions of each particle type; representative spICP-TOFMS time traces and mass spectra of each particle type; mass correlation of Ti and Nb in rutile, ilmenite and biotite; mass correlation of Fe and Al with Ti in ilmenite and biotite; particle size distribution of E171 and Ti-nat particles; false-positive, true positive and false-negative classifications for rutile and E171 (Ti-eng) particles as a function of the Ti:Nb mass ratio; multi-isotope calibration strategy for quantification of Ti; quantitative analysis of Ti-nat particles; quantitative analysis of E171 particles in stream water; recovery of classified Ti-eng (E171) particles in stream water

Conflicts of interest

The authors do not have any conflicts of interest to declare.

Acknowledgements

The authors would like to acknowledge Iowa State University for faculty start-up grant and partial funding though NSF CAREER grant CHE-2237291. We also like to acknowledge Ed Raines, curator of the Mines Museum of Earth Science, as well as Dr. James Ranville and Aaron Goodman from Colorado School of Mines, for providing Ti-mineral samples. We also acknowledge the ISU glass and machine shop for the construction of microdroplet introduction assembly.

References

1. Giese, B.; Klaessig, F.; Park, B.; Kaegi, R.; Steinfeldt, M.; Wigger, H.; von Gleich, A.; Gottschalk, F., Risks, Release and Concentrations of Engineered Nanomaterial in the Environment. *Sci Rep* **2018,** *8* (1), 1-18.
2. Hassellöv, M.; Kaegi, R., Analysis and characterization of manufactured nanoparticles in aquatic environments. Environmental and human health impacts of nanotechnology. *John Wiley & Sons, Ltd* **2009**, 211-266.
3. Erhardt, T.; Jensen, C. M.; Borovinskaya, O.; Fischer, H., Single Particle Characterization and Total Elemental Concentration Measurements in Polar Ice Using Continuous Flow Analysis-Inductively Coupled Plasma Time-of-Flight Mass Spectrometry. *Environ Sci Technol* **2019,** *53* (22), 13275-13283.
4. Nishiguchi, K.; Utani, K.; Fujimori, E., Real-time multielement monitoring of airborne particulate matter using ICP-MS instrument equipped with gas converter apparatus. *J. Anal. At. Spectrom.* **2008,** *23* (8), 1125-1129.
5. Pósfai, M.; Buseck, P. R., Nature and Climate Effects of Individual Tropospheric Aerosol Particles. *Annual Review of Earth and Planetary Sciences* **2010,** *38* (1), 17-43.
6. Hochella, M. F., Jr.; Mogk, D. W.; Ranville, J.; Allen, I. C.; Luther, G. W.; Marr, L. C.; McGrail, B. P.; Murayama, M.; Qafoku, N. P.; Rosso, K. M.; Sahai, N.; Schroeder, P. A.; Vikesland, P.; Westerhoff, P.; Yang, Y., Natural, incidental, and engineered nanomaterials and their impacts on the Earth system. *Science* **2019,** *363* (6434).
7. Hochella, M. F. J.; Lower, S. K.; Maurice, P. A.; Penn, R. L.; Sahai, N.; Sparks, D. L.; Twining, B. S., Nanominerals, Mineral Nanoparticles,and Earth Systems. *Science* **2008,** *319* (5870), 1631-1635.
8. USGS, National Minerals Information Center, Titanium Statistics and Information. https://www.usgs.gov/centers/nmic/titanium-statistics-and-information (accessed 2022-08-01).

9. Yaroshevsky, A. A., Abundances of chemical elements in the Earth's crust. *Geochemistry International* **2006,** *44* (1), 48-55.
10. Braun, H.; Baidins, A.; Marganski, R. E., TiO_2 pigment technology: A Review. *Prog. Organic Coat* **1992,** *20*, 105-138.
11. Nakata, K.; Fujishima, A., TiO_2 photocatalysis: Design and applications. *Journal of Photochemistry and Photobiology C: Photochemistry Reviews* **2012,** *13* (3), 169-189.
12. Galletti, A.; Seo, S.; Joo, S. H.; Su, C.; Blackwelder, P., Effects of titanium dioxide nanoparticles derived from consumer products on the marine diatom Thalassiosira pseudonana. *Environ Sci Pollut Res Int* **2016,** *23* (20), 21113-21122.
13. Weir, A.; Westerhoff, P.; Fabricius, L.; Hristovski, K.; von Goetz, N., Titanium dioxide nanoparticles in food and personal care products. *Environ Sci Technol* **2012,** *46* (4), 2242-50.
14. Popov, A. P.; Priezzhev, A. V.; Lademann, J.; Myllylä, R., TiO_2 nanoparticles as an effective UV-B radiation skin-protective compound in sunscreens. *Journal of Physics D: Applied Physics* **2005,** *38* (15), 2564-2570.
15. Lan, Y.; Lu, Y.; Ren, Z., Mini review on photocatalysis of titanium dioxide nanoparticles and their solar applications. *Nano Energy* **2013,** *2* (5), 1031-1045.
16. Loosli, F.; Wang, J.; Rothenberg, S.; Bizimis, M.; Winkler, C.; Borovinskaya, O.; Flamigni, L.; Baalousha, M., Sewage spills are a major source of titanium dioxide engineered (nano)-particles into the environment. *Environ Sci Nano* **2019,** *6* (3), 763-777.
17. Keller, A. A.; Lazareva, A., Predicted Releases of Engineered Nanomaterials: From Global to Regional to Local. *Environmental Science & Technology Letters* **2013,** *1* (1), 65-70.
18. Gottschalk, F.; Sonderer, T.; Scholz, R. W.; Nowack, B., Modeled Environmental Concentrations of Engineered Nanomaterials (TiO2, ZnO, Ag, CNT, Fullerenes) for Different Regions. *Environ Sci Technol* **2009,** *43(24)*, 9216–9222.
19. Phalyvong, K.; Sivry, Y.; Pauwels, H.; Gélabert, A.; Tharaud, M.; Wille, G.; Bourrat, X.; Ranville, J. F.; Benedetti, M. F., Assessing CeO2 and TiO2 Nanoparticle Concentrations in the Seine River and Its Tributaries Near Paris. *Frontiers in Environmental Science* **2021,** *8*, 271.
20. Sun, T. Y.; Gottschalk, F.; Hungerbühler, K.; Nowack, B., Comprehensive probabilistic modelling of environmental emissions of engineered nanomaterials. *Environ. Pollut.* **2014,** *185*, 69-76.
21. Coll, C.; Notter, D.; Gottschalk, F.; Sun, T.; Som, C.; Nowack, B., Probabilistic environmental risk assessment of five nanomaterials (nano-TiO2, nano-Ag, nano-ZnO, CNT, and fullerenes). *Nanotoxicology* **2016,** *10* (4), 436-444.
22. Garner, K. L.; Suh, S.; Keller, A. A., Assessing the Risk of Engineered Nanomaterials in the Environment: Development and Application of the nanoFate Model. *Environ. Sci. Technol.* **2017,** *51* (10), 5541-5551.
23. Mueller, N. C.; Nowack, B., Exposure Modeling of Engineered Nanoparticles in the Environment. *Environ. Sci. Technol.* **2008,** *42* (12), 4447-4453.
24. Zheng, Y.; Nowack, B., Size-Specific, Dynamic, Probabilistic Material Flow Analysis of Titanium Dioxide Releases into the Environment. *Environ. Sci. Technol.* **2021,** *55* (4), 2392-2402.
25. European Chemicals Bureau 2008.Technical Guidance Document on Risk Assessment. Available online at: https://echa.europa.eu/documents/10162/13632/information_requirements_r10_en.pdf/bb902be7-a503-4ab7-9036-d866b8ddce69.
26. Danovaro, R.; Bongiorni, L.; Corinaldesi, C.; Giovannelli, D.; Damiani, E.; Astolfi, P.; Greci, L.; Pusceddu, A., Sunscreens cause coral bleaching by promoting viral infections. *Environ Health Perspect* **2008,** *116* (4), 441-447.
27. Zhu, X.; Zhou, J.; Cai, Z., TiO2 nanoparticles in the marine environment: impact on the toxicity of tributyltin to abalone (Haliotis diversicolor supertexta) embryos. *Environ Sci Technol* **2011,** *45* (8), 3753-3758.

28. Rihane, N.; Nury, T.; M'Rad, I.; El Mir, L.; Sakly, M.; Amara, S.; Lizard, G., Microglial cells (BV-2) internalize titanium dioxide (TiO2) nanoparticles: toxicity and cellular responses. *Environ Sci Pollut Res Int* **2016,** *23* (10), 9690-9699.
29. Baan, R.; Straif, K.; Grosse, Y.; Secretan, B.; El Ghissassi, F.; Cogliano, V., Carcinogenicity of carbon black, titanium dioxide, and talc. *The Lancet Oncology* **2006,** *7* (4), 295-296.
30. EFSA FAF Panel (EFSA Panel on Food Additives and Flavourings); Younes, M.; Aquilina, G.; Castle, L.; Engel, K.-H.; Fowler, P.; Frutos Fernandez, M. J.; Fürst, P.; Gundert-Remy, U.; Gürtler, R.; Husøy, T.; Manco, M.; Mennes, W.; Moldeus, P.; Passamonti, S.; Shah, R.; Waalkens-Berendsen, I.; Wölfle, D.; Corsini, E.; Cubadda, F.; De Groot, D.; FitzGerald, R.; Gunnare, S.; Gutleb, A. C.; Mast, J.; Mortensen, A.; Oomen, A.; Piersma, A.; Plichta, V.; Ulbrich, B.; Van Loveren, H.; Benford, D.; Bignami, M.; Bolognesi, C.; Crebelli, R.; Dusinska, M.; Marcon, F.; Nielsen, E.; Schlatter, J.; Vleminckx, C.; Barmaz, S.; Carfí, M.; Civitella, C.; Giarola, A.; Rincon, A. M.; Serafimova, R.; Smeraldi, C.; Tarazona, J.; Tard, A.; Wright, M., Safety assessment of titanium dioxide (E171) as a food additive. *EFSA Journal* **2021,** *19* (5), e06585.
31. Hoo, C. M.; Starostin, N.; West, P.; Mecartney, M. L., A comparison of atomic force microscopy (AFM) and dynamic light scattering (DLS) methods to characterize nanoparticle size distributions. *Journal of Nanoparticle Research* **2008,** *10* (S1), 89-96.
32. Plathe, K. L.; von der Kammer, F.; Hassellöv, M.; Moore, J.; Murayama, M.; Hofmann, T.; Hochella, M. F., Using FlFFF and aTEM to determine trace metal–nanoparticle associations in riverbed sediment. *Environmental Chemistry* **2010,** *7* (1), 82-93.
33. Gray, E. P.; Bruton, T. A.; Higgins, C. P.; Halden, R. U.; Westerhoff, P.; Ranville, J. F., Analysis of gold nanoparticle mixtures: a comparison of hydrodynamic chromatography (HDC) and asymmetrical flow field-flow fractionation (AF4) coupled to ICP-MS. *J. Anal. At. Spectrom.* **2012,** *27* (9), 1532-1539.
34. Kammer, F. v. d.; Legros, S.; Hofmann, T.; Larsen, E. H.; Loeschner, K., Separation and characterization of nanoparticles in complex food and environmental samples by field-flow fractionation. *TrAC, Trends Anal. Chem.* **2011,** *30* (3), 425-436.
35. Stolpe, B.; Hassellöv, M.; Andersson, K.; Turner, D. R., High resolution ICPMS as an on-line detector for flow field-flow fractionation; multi-element determination of colloidal size distributions in a natural water sample. *Analytica Chimica Acta* **2005,** *535* (1-2), 109-121.
36. Bojeong, K.; Park, C.-S.; Murayama, M.; Hochella, M. F., Discovery and characterization of Silver Sulfide Nanoparticles in final sewage sludge products. *Environmental science & Technology* **2010,** *44*, 7509-7514.
37. Kim, B. G.; Kang, I. J., Evaluation of the effects of biodegradable nanoparticles on a vaccine delivery system using AFM, SEM, and TEM. *Ultramicroscopy* **2008,** *108* (10), 1168-73.
38. Gondikas, A. P.; von der Kammer, F.; Reed, R. B.; Wagner, S.; Ranville, J. F.; Hofmann, T., Release of TiO2 nanoparticles from sunscreens into surface waters: a one-year survey at the old Danube recreational Lake. *Environ Sci Technol* **2014,** *48* (10), 5415-5422.
39. Degueldre, C.; Favarger, P. Y., Colloid analysis by single particle inductively coupled plasma-mass spectroscopy: a feasibility study. *Colloids and Surfaces A: Physicochemical and Engineering Aspects* **2003,** *217* (1-3), 137-142.
40. Lee, W.-W.; Chan, W.-T., Calibration of single-particle inductively coupled plasma-mass spectrometry (SP-ICP-MS). *J. Anal. At. Spectrom.* **2015,** *30* (6), 1245-1254.
41. Olesik, J. W.; Gray, P. J., Considerations for measurement of individual nanoparticles or microparticles by ICP-MS: determination of the number of particles and the analyte mass in each particle. *Journal of Analytical Atomic Spectrometry* **2012,** *27* (7), 1143-1155.
42. Kocic, J.; Günther, D.; Hattendorf, B., Improving detection capability for single particle inductively coupled plasma mass spectrometry with microdroplet sample introduction. *J. Anal. At. Spectrom.* **2021,** *36* (1), 233-242.

43. Montaño, M. D.; Badiei, H. R.; Bazargan, S.; Ranville, J. F., Improvements in the detection and characterization of engineered nanoparticles using spICP-MS with microsecond dwell times. *Environ. Sci.: Nano* **2014,** *1* (4), 338-346.
44. Ding, K.; Liang, S.; Xie, C.; Wan, Q.; Jin, C.; Wang, S.; Tang, Y. T.; Zhang, M.; Qiu, R., Discrimination and Quantification of Soil Nanoparticles by Dual-Analyte Single Particle ICP-QMS. *Anal Chem* **2022,** *94* (30), 10745-10753.
45. Borovinskaya, O.; Hattendorf, B.; Tanner, M.; Gschwind, S.; Günther, D., A prototype of a new inductively coupled plasma time-of-flight mass spectrometer providing temporally resolved, multi-element detection of short signals generated by single particles and droplets. *J. Anal. At. Spectrom.* **2013,** *28* (2), 226-233.
46. Borovinskaya, O.; Gschwind, S.; Hattendorf, B.; Tanner, M.; Gunther, D., Simultaneous mass quantification of nanoparticles of different composition in a mixture by microdroplet generator-ICPTOFMS. *Anal Chem* **2014,** *86* (16), 8142-8.
47. Hendriks, L.; Gundlach-Graham, A.; Hattendorf, B.; Günther, D., Characterization of a new ICP-TOFMS instrument with continuous and discrete introduction of solutions. *J. Anal. At. Spectrom.* **2017,** *32* (3), 548-561.
48. Praetorius, A.; Gundlach-Graham, A.; Goldberg, E.; Fabienke, W.; Navratilova, J.; Gondikas, A.; Kaegi, R.; Günther, D.; Hofmann, T.; von der Kammer, F., Single-particle multi-element fingerprinting (spMEF) using inductively-coupled plasma time-of-flight mass spectrometry (ICP-TOFMS) to identify engineered nanoparticles against the elevated natural background in soils. *Environ. Sci.: Nano* **2017,** *4* (2), 307-314.
49. Bland, G. D.; Zhang, P.; Valsami-Jones, E.; Lowry, G. V., Application of Isotopically Labeled Engineered Nanomaterials for Detection and Quantification in Soils via Single-Particle Inductively Coupled Plasma Time-of-Flight Mass Spectrometry. *Environ Sci Technol* **2022,** *56* (22), 15584-15593.
50. Nabi, M. M.; Wang, J.; Goharian, E.; Baalousha, M., Temporal variation in TiO_2 engineered particle concentrations in the Broad River during dry and wet weathers. *Sci Total Environ* **2022,** *807* (Pt 3), 151081.
51. Tou, F.; Nabi, M. M.; Wang, J.; Erfani, M.; Goharian, E.; Chen, J.; Yang, Y.; Baalousha, M., Multi-method approach for analysis of road dust particles: elemental ratios, SP-ICP-TOF-MS, and TEM. *Environmental Science: Nano* **2022,** *9* (10), 3859-3872.
52. Mehrabi, K.; Kaegi, R.; Gunther, D.; Gundlach-Graham, A., Emerging investigator series: automated single-nanoparticle quantification and classification: a holistic study of particles into and out of wastewater treatment plants in Switzerland. *Environ Sci Nano* **2021,** *8* (5), 1211-1225.
53. Brunjes, R.; Schuurman, J.; Kammer, F. V.; Hofmann, T., Rapid analysis of gunshot residues with single-particle inductively coupled plasma time-of-flight mass spectrometry. *Forensic Sci Int* **2022,** *332*, 111202.
54. Pradas del Real, A. E.; Castillo-Michel, H.; Kaegi, R.; Larue, C.; de Nolf, W.; Reyes-Herrera, J.; Tucoulou, R.; Findling, N.; Salas-Colera, E.; Sarret, G., Searching for relevant criteria to distinguish natural vs. anthropogenic TiO2 nanoparticles in soils. *Environ. Sci.: Nano* **2018,** *5* (12), 2853-2863.
55. Slomberg, D. L.; Auffan, M.; Guéniche, N.; Angeletti, B.; Campos, A.; Borschneck, D.; Aguerre-Chariol, O.; Rose, J., Anthropogenic Release and Distribution of Titanium Dioxide Particles in a River Downstream of a Nanomaterial Manufacturer Industrial Site. *Frontiers in Environmental Science* **2020,** *8* (76).
56. Bland, G. D.; Battifarano, M.; Pradas Del Real, A. E.; Sarret, G.; Lowry, G. V., Distinguishing Engineered TiO2 Nanomaterials from Natural Ti Nanomaterials in Soil Using spICP-TOFMS and Machine Learning. *Environ Sci Technol* **2022,** *56* (5), 2990-3001.
57. Force, E. R.; Force, E. R., Geology of Titanium-Mineral Deposits. In *Geology of Titanium-Mineral Deposits*, Geological Society of America: 1991; Vol. 259, p 0.

58. Mehrabi, K.; Günther, D.; Gundlach-Graham, A., Single-particle ICP-TOFMS with online microdroplet calibration for the simultaneous quantification of diverse nanoparticles in complex matrices. *Environ. Sci.: Nano* **2019,** *6* (11), 3349-3358.
59. Harycki, S.; Gundlach-Graham, A., Online microdroplet calibration for accurate nanoparticle quantification in organic matrices. *Anal Bioanal Chem* **2022,** *414* (25), 7543-7551.
60. Gundlach-Graham, A.; Mehrabi, K., Monodisperse microdroplets: a tool that advances single-particle ICP-MS measurements. *J. Anal. At. Spectrom.* **2020,** *35* (9), 1727-1739.
61. Currie, L. A., Nomenclature in evaluation of analytical methods including detection and quantification capabilities. *Pure Appl. Chem.* **1995,** *67*, 1699-1723.
62. Gundlach-Graham, A.; Hendriks, L.; Mehrabi, K.; Gunther, D., Monte Carlo Simulation of Low-Count Signals in Time-of-Flight Mass Spectrometry and Its Application to Single-Particle Detection. *Anal Chem* **2018,** *90* (20), 11847-11855.
63. Gundlach-Graham, A.; Lancaster, R., Mass-Dependent Critical Value Expressions for Particle Finding in Single-Particle ICP-TOFMS. *Anal. Chem.* **2023,** *95* (13), 5618-5626.
64. Harycki, S.; Gundlach-Graham, A., Characterization of a high-sensitivity ICP-TOFMS instrument for microdroplet, nanoparticle, and microplastic analyses. *J. Anal. At. Spectrom.* **2022,** *38* (1), 111-120.
65. Biotite, http://www.webmineral.com/data/Biotite.shtml#.Y3e9_3bMJaR (accessed November, 2022).
66. Ilmenite, https://www.mindat.org/min-2013.html (accessed November, 2022).
67. Rutile, https://www.mindat.org/min-3486.html (accessed November, 2022).
68. Szakas, S. E.; Lancaster, R.; Kaegi, R.; Gundlach-Graham, A., Quantification and classification of engineered, incidental, and natural cerium-containing particles by spICP-TOFMS. *Environ. Sci.: Nano* **2022,** *9* (5), 1627-1638.
69. Currie, L. A., Limits for quantiative detection and quantitative determination. Application to radiochemistry. *Analytical Chemistry* **1968,** *40*, 586-593.
70. Triebold, S.; Luvizotto, G. L.; Tolosana-Delgado, R.; Zack, T.; von Eynatten, H., Discrimination of TiO2 polymorphs in sedimentary and metamorphic rocks. *Contributions to Mineralogy and Petrology* **2010,** *161* (4), 581-596.
71. Plavsa, D.; Reddy, S. M.; Agangi, A.; Clark, C.; Kylander-Clark, A.; Tiddy, C. J., Microstructural, trace element and geochronological characterization of TiO2 polymorphs and implications for mineral exploration. *Chemical Geology* **2018,** *476*, 130-149.
72. Pinto, A. J.; Sanchez-Pastor, N.; Callegari, I.; Pracejus, B.; Scharf, A., Challenges to rutile-based geoscientific tools: low-temperature polymorphic TiO(2) transformations and corresponding reactive pathways. *Sci Rep* **2020,** *10* (1), 7445.
73. Zack, T.; Kronz, A.; Foley, S. F.; Rivers, T., Trace element abundances in rutiles from eclogites and associated garnet mica schists. *Chemical Geology* **2002,** *184* (1), 97-122.
74. Goodman, A. J.; Gundlach-Graham, A.; Bevers, S. G.; Ranville, J. F., Characterization of nano-scale mineral dust aerosols in snow by single particle inductively coupled plasma mass spectrometry. *Environ. Sci.: Nano* **2022,** *9* (8), 2638-2652.
75. Erhardt, T.; Jensen, C. M.; Borovinskaya, O.; Fischer, H., Single Particle Characterization and Total Elemental Concentration Measurements in Polar Ice Using Continuous Flow Analysis-Inductively Coupled Plasma Time-of-Flight Mass Spectrometry. *Environ. Sci. Technol.* **2019,** *53* (22), 13275-13283.
76. Nabi, M. M.; Wang, J.; Erfani, M.; Goharian, E.; Baalousha, M., Urban runoff drives titanium dioxide engineered particle concentrations in urban watersheds: field measurements. *Environ. Sci.: Nano* **2023,** *10* (3), 718-731.